Journal of Rock Mechanics and Geotechnical Engineering 7 (2015) 327–336

Contents lists available at ScienceDirect

Journal of Rock Mechanics and Geotechnical Engineering

journal homepage: www.rockgeotech.org

Full length article

DEM investigation of weathered rocks using a novel bond contact model

Zhenming Shi [a,b], Tao Jiang [a,b], Mingjing Jiang [a,b,c,*], Fang Liu [a,b,c], Ning Zhang [a,b]

[a] Department of Geotechnical Engineering, College of Civil Engineering, Tongji University, Shanghai, 200092, China
[b] Key Laboratory of Geotechnical and Underground Engineering of Ministry of Education, Tongji University, Shanghai, 200092, China
[c] State Key Laboratory for Disaster Reduction in Civil Engineering, Tongji University, Shanghai, 200092, China

ARTICLE INFO

Article history:
Received 20 August 2014
Received in revised form
16 October 2014
Accepted 12 January 2015
Available online 26 March 2015

Keywords:
Distinct element method (DEM)
Bond contact model
Rock weathering
Weathering law
Microscopic parameter

ABSTRACT

The distinct element method (DEM) incorporated with a novel bond contact model was applied in this paper to shed light on the microscopic physical origin of macroscopic behaviors of weathered rock, and to achieve the changing laws of microscopic parameters from observed decaying properties of rocks during weathering. The changing laws of macroscopic mechanical properties of typical rocks were summarized based on the existing research achievements. Parametric simulations were then conducted to analyze the relationships between macroscopic and microscopic parameters, and to derive the changing laws of microscopic parameters for the DEM model. Equipped with the microscopic weathering laws, a series of DEM simulations of basic laboratory tests on weathered rock samples was performed in comparison with analytical solutions. The results reveal that the relationships between macroscopic and microscopic parameters of rocks against the weathering period can be successfully attained by parametric simulations. In addition, weathering has a significant impact on both stress–strain relationship and failure pattern of rocks.

1. Introduction

Weathering of rocks is a process of the disintegration of rocks through contact with the Earth's atmosphere, biota and water. Weathering is common in nature and may deteriorate not only physical properties of rocks (e.g. density, void ratio, and hydraulic properties), but also the mechanical properties (e.g. reduction in strength over time). Hence, it is of great significance to understand the long-term mechanical behavior of rocks to achieve economically and mechanically adequate designs for structures involving rock masses in the entire life cycle, such as high rock slopes, and underground radioactive waste deposit.

Presently, the phenomenon of rock weathering has been extensively studied using experimental approaches, which, however, fail to determine the weathering time due to the long-time span and the error from dating methods. Instead, degree of weathering is generally used for classification. Gupta and Rao (1998, 2000) investigated the physico-mechanical properties of rocks under different degrees of weathering and presented the relations between the indices. Tugrul (2004), Beavis et al. (1982), and Irfan and Dearman (1978) also experimentally studied the physico-mechanical properties of a variety of weathered rocks classified by the degree of weathering.

Merely a minority of researchers estimated the weathering time using isotopic dating method. Sunamura (1996) summarized the rate of coastal tafoni development. Hachinohe et al. (2000) studied the rate at which the thicknesses of weathered zones increase and the strengths of weathered rocks decrease. Based on this work, they proposed an approach for predicting rock strength at a given depth and weathering time. In addition, Oguchi et al. (1999) examined four dated lava domes made of porous rhyolite and performed a series of experimental tests to investigate the evolution rules of rock properties, and Matsukura et al. (2002) investigated the same material with emphasis on the effect of weathering on strength anisotropy.

The aforementioned efforts have demonstrated that the weathering process impacts not only the strengths of rocks, but also their deformation behaviors. The authors believe that the variations of rock behaviors are closely related to the change of microstructure and micro-properties. However, it is still extremely difficult to detect the evolution of microstructure during weathering using any available experimental technique. Alternatively, the distinct element method (DEM) equipped with a proper bond contact model for rocks stands out as a powerful tool to study the

* Corresponding author. Tel.: +86 21 65980238; fax: +86 21 65985210.
E-mail address: mingjing.jiang@tongji.edu.cn (M. Jiang).

Peer review under responsibility of Institute of Rock and Soil Mechanics, Chinese Academy of Sciences.
1674-7755
http://dx.doi.org/10.1016/j.jrmge.2015.01.005

macroscopic and microscopic characteristics of weathered rocks. This approach was originally proposed by Cundall and Strack (1979) based on the discrete mechanics, and is widely applied in the field of geotechnical engineering due to its capacity of modeling heterogeneous, discontinuous materials subjected to large deformation and related macroscopic behaviors with microscopic mechanisms. Recently, the method has been introduced into the field of rock mechanics and shows a great potential. Potyondy and Cundall (2004) proposed the bonded particle model (BPM) to model Lac du Bonnet granite. Wang and Tonon (2009) subsequently proposed the three-dimensional (3D) bond model to study the triaxial behaviors of the same material. Jiang et al. (2013) developed a novel bond contact model for rocks on the basis of experimental investigation and theoretical analysis, and reproduced adequately the mechanical behaviors of typical rocks such as the Lac du Bonnet granite.

Several researchers made valuable contributions to DEM analyses of rock weathering. Calvetti et al. (2005) modeled the degradation of strength due to weathering by means of continuous and discrete approaches. Utili and Nova (2008) established a contact bond model based on two micromechanical contributions (i.e. intergranular friction and cohesive bond force) and modeled the evolution of natural cliffs subjected to weathering as an example. However, the evolution of rock strength applied in the study was based on the research conducted by Kimmance (1988), where the strength was not related to weathering time, resulting in an unclear relationship between rock slope stability and time period. Nevertheless, these studies remain preliminary by using simple contact models of rocks.

In this paper, time-dependent weathering laws were established for rock mechanical properties (strength and deformation parameters), and their relations with the evolution of microscopic parameters were investigated by deploying a novel contact model for rocks (Jiang et al., 2013). This study aims to enhance the understanding of weathering of rocks from a microscopic point of view, and to promote future investigations including rock properties prediction and practical engineering modeling. Although this paper presents the results derived from porous rhyolite as an example, the presented methodology and qualitative relationship are applicable to other types of rocks weathered in different circumstances.

2. Evolution laws of macroscopic mechanical properties of rocks due to weathering

Although weathering may give rise to a variety of changes on rocks, this paper regards the degradation of rock mechanical properties as the overall impact of weathering on the basis of available research findings without distinguishing different mechanisms. Oguchi et al. (1999) performed a series of unconfined compression tests and Brazilian tests on the porous rhyolite subjected to different weathering times over 40 thousand years, and the strengths obtained against the weathering time are listed in Table 1.

In the light of the formula presented by Sunamura (1996), an exponential function ($y = ae^{-bx}$) is selected to fit the experimental data. The relationships between normalized strengths and weathering time are shown in Fig. 1, and the corresponding equations are given as follows:

$$\sigma_c/\sigma_{c0} = e^{-0.0404t} \quad (1)$$

$$\sigma_t/\sigma_{t0} = e^{-0.0643t} \quad (2)$$

where σ_c is the unconfined compressive strength (MPa); σ_t is the tensile strength (MPa); σ_{c0} and σ_{t0} are the maximum compressive and tensile strengths (MPa), respectively; and t is the weathering time (ka).

Fig. 1 shows that rock strengths decrease significantly at the initial stage of weathering, and the degradation rate decreases with increasing weathering time, which can be adequately captured by the exponential function. Besides, the degradation rate of tensile strength is greater than that of compressive strength. It is noted that although both lithology and weathering environment may impact the behaviors of weathered rock, the general trend can be featured by the same function with different fitting constants.

Unfortunately, Oguchi et al. (1999) provided no experimental data of deformation parameters. Thus, the experimental observation reported by Gupta and Rao (2000) is used instead to establish the evolution law of deformation parameters. They tested strengths, elastic modulus and Poisson's ratio of weathered granite, basalt and quartzite at different weathering grades. In this study, we select the data of basalt and estimate the weathering times for each weathering grade using Eqs. (1) and (2), assuming the same weathering laws as porous rhyolite (Table 2). Although two different calculated values can be obtained from Eq. (1) or Eq. (2), the discrepancy is small and the adjusted value is observed to fit both curves of Eqs. (1) and (2) (Fig. 2).

Table 1
Compressive and tensile strengths of porous rhyolite at different weathering times (Oguchi et al., 1999).

Weathering time (ka)	Compressive strength (MPa)	Tensile strength (MPa)
1.1	15.3	1.97
2.6	13.7	2.11
20	5.9	0.47
40	4	0.24

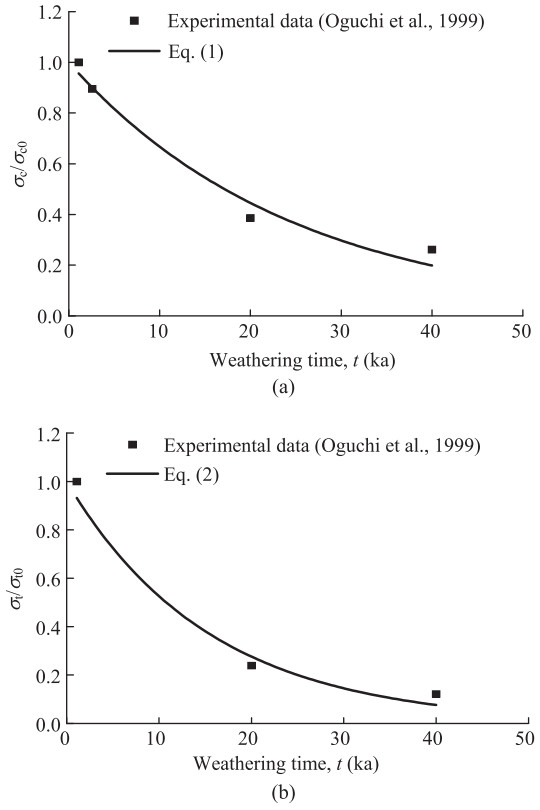

Fig. 1. Evolution laws of (a) unconfined compressive strength and (b) tensile strength.

Table 2
Mechanical properties of basalt at different weathering grades (Gupta and Rao, 2000).

Weathering grade	Tensile strength (MPa)	Compressive strength (MPa)	Tangent modulus (GPa)	Poisson's ratio	Estimated weathering time (ka)
BW0	27.46	172.55	46.51	0.19	0
BW1	16.25	93.2	20.63	0.26	12
BW3	1.9	17.8	2.77	0.27	50
BW4	0.21	3.4	0.63	–	95

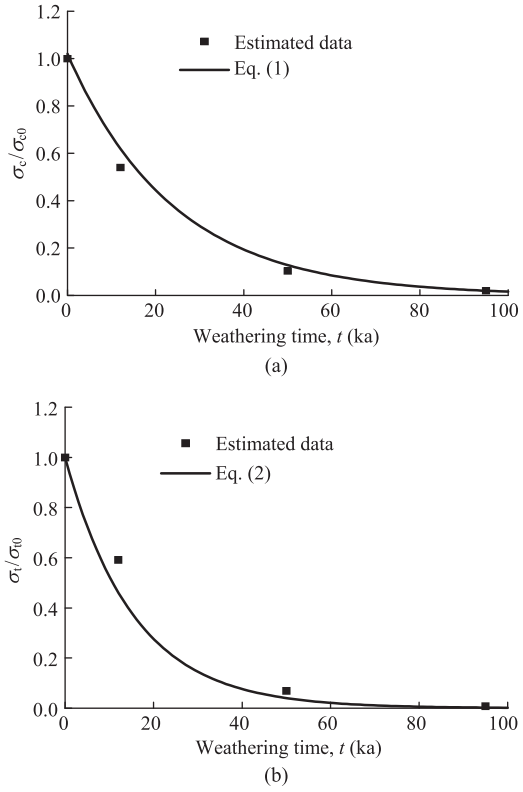

Fig. 2. Estimated data and calculated results in terms of (a) unconfined compressive strength and (b) tensile strength.

The estimated weathering times are applied to summarize the changing laws of elastic modulus and Poisson's ratio. As shown in Fig. 3, an exponential function is suitable for fitting the changing laws of elastic modulus, while a linear approximation is acceptable in terms of Poisson's ratio due to the lack of data and the small range of variation. The corresponding equations are as follows:

$$E/E_0 = e^{-0.066t} \quad (3)$$

$$\nu = 0.19 + 5.83 \times 10^{-3} t \quad (t < 12 \text{ ka}) \quad (4)$$

where E is the elastic modulus (GPa), E_0 is the maximum elastic modulus (GPa) in the corresponding set of tests, and ν is the Poisson's ratio.

3. Changing laws of microscopic properties in DEM analyses

3.1. Outline of the DEM bond contact model

The bond contact model used in this study was developed for rocks on the basis of experimental investigation and theoretical

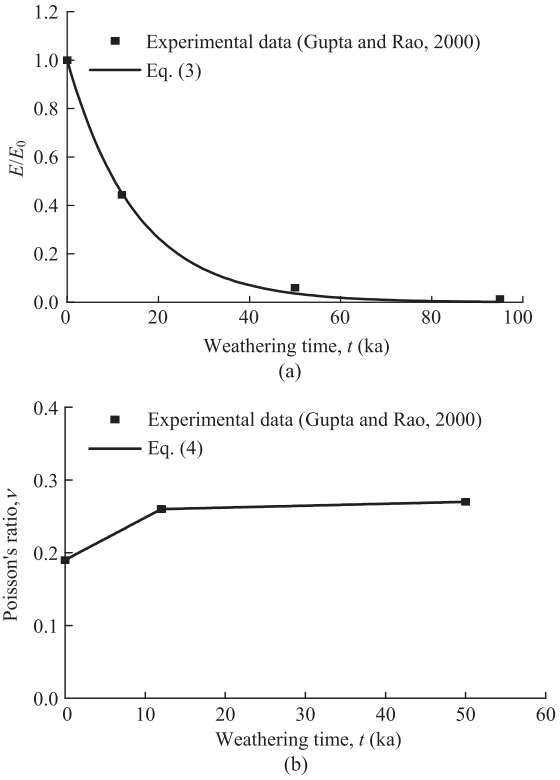

Fig. 3. Changing laws of (a) normalized elastic modulus and (b) Poisson's ratio.

analysis. More details of the model can be found in Jiang et al. (2013), and only several significant features of the model are recapped here for completeness.

Fig. 4 presents a simplified illustration of the bond contact model, which is functioned by dashpots, springs and bond elements in normal, tangential, and rolling directions, respectively. This model was developed by Jiang et al. (2006, 2012) through theoretical derivation and experimental research. Fig. 5 shows the mechanical responses of the model in normal, tangential and rolling directions, where the inflexion points represent the failure of the bond and the consequent loss of strength. The bond strength envelope used in the models, as shown in Fig. 6, was obtained

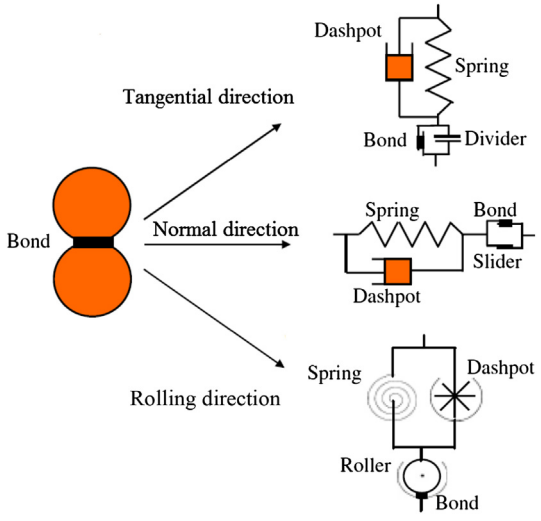

Fig. 4. Illustration of the bond contact model (after Jiang et al., 2006).

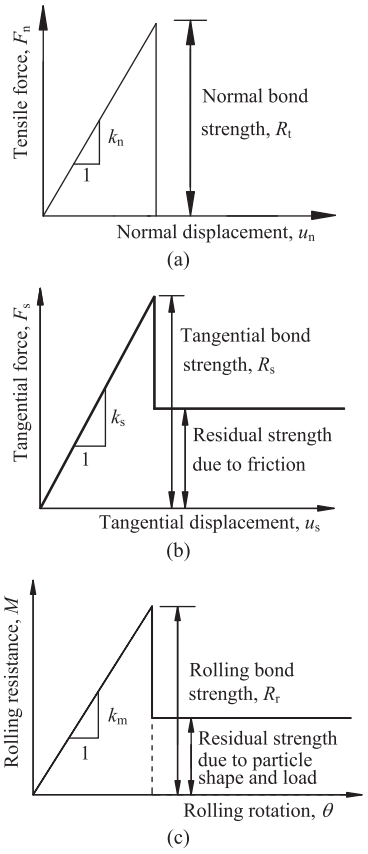

Fig. 5. Schematic illustration of the mechanical responses of the bond contact model in (a) normal direction, (b) tangential direction, and (c) rolling direction (Jiang et al., 2006, 2012).

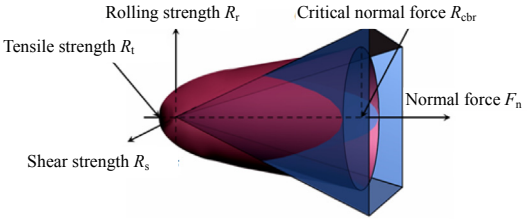

Fig. 6. Strength envelope for cemented geomaterials.

through a series of laboratory tests. A bond will irreversibly break once its contact forces reach the strength envelope, where the parabolic section represents the peak strength provided by the bond and the planar section represents the residual strength due to friction. This model has been proved to be more rigorous for rocks than other existing models (e.g. BPM and clumped particle model) by comparing the simulated mechanical behaviors with the experimental results (Jiang et al., 2013).

3.2. Preparation of DEM rock sample

In DEM modeling, the macroscopic responses of the material are dominated by the contact model, particle size and its distribution, and the microscopic parameters. The particle size distribution (PSD) and the initial void ratio of the rock sample in this study were presented by Jiang et al. (2013), which were originally selected for Lac du Bonnet granite, and the strength and stiffness parameters assigned to the bond contact model were calibrated on a trial-and-

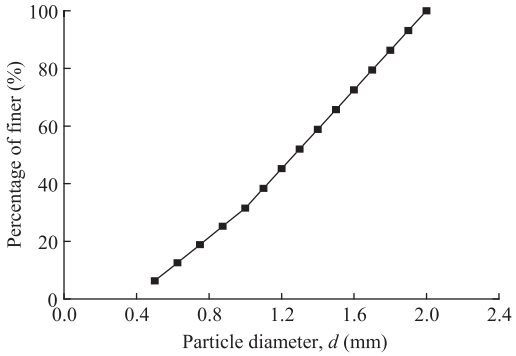

Fig. 7. Particle size distribution (PSD) used in the DEM analyses.

error basis so as to reproduce the macro-responses of the target rock. It should be noted that the PSD will affect the mechanical properties of rocks in combination with other factors. The same results could be achieved by simultaneously changing the PSD and the other model parameters based on inverse analysis. If the PSD is changed while the other parameters remain unchanged, this may lead to different behaviors of rocks. The pure effect of the PSD has been revealed in some literature (e.g. Morgan, 1999; Shimizu et al., 2011; Minh and Cheng, 2013; Wiącek and Molenda, 2014), which, however, is beyond the scope of this paper.

In this study, 15 particle sizes are considered, with the maximum and minimum diameters of 2 mm and 0.5 mm, respectively, and the average diameter is 1.3 mm (Fig. 7). A total of 10,000 particles were firstly generated and compacted using the multilayer under-compaction method (Jiang et al., 2003) to achieve a uniform rectangular sample with the size of 13.8 cm × 6.9 cm. Bonds were subsequently assigned to the contacts during the vertical consolidation process, in which a vertical stress of 529 kPa was applied by moving top and bottom rigid walls towards each other. The generated DEM rock sample for the uniaxial compression tests is shown in Fig. 8a, and the sample for direct tension tests is processed by partially removing particles (Fig. 8b). The unchanged microscopic parameters of the initial samples are listed in Table 3.

3.3. Relationships between macroscopic and microscopic parameters

A parametric study of DEM simulation of uniaxial compression tests and direct tension tests was conducted to feature the evolution laws of the microscopic parameters according to the observed

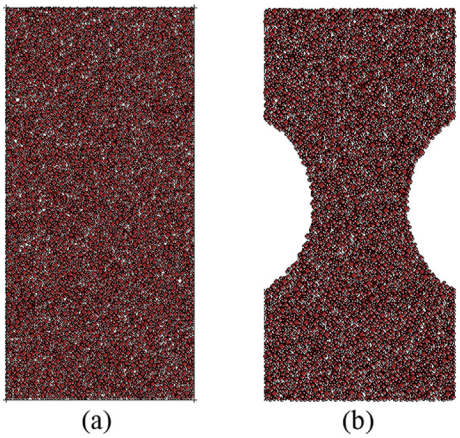

Fig. 8. DEM rock samples for (a) uniaxial compression test and (b) direct tension test.

Table 3
Microscopic parameters of the initial rock samples (Jiang et al., 2013).

Particle density (kg m^{-3})	Inter-particle friction coefficient, μ_p	Inter-particle rolling resistance coefficient, β_p	Inter-bond friction coefficient of bonds, μ_b	Inter-bond rolling resistance coefficient, β_b
2700	1	1.5	0.5	0.5

degradation of rock properties. It is noted that the particle stiffnesses, bond strengths and stiffnesses are the key microscopic parameters being investigated here.

Simulations reveal that stiffness parameters are independent of strength parameters and thus are firstly analyzed. According to Griffiths and Mustoe (2001), the relationship between ratio of elastic modulus to tangential stiffness (E/k_s) and stiffness ratio (i.e. k_s/k_n), and that between Poisson's ratio (ν) and the stiffness ratio, are established. The simulation results are shown in Fig. 9 and the expressions are shown as follows:

$$\frac{E}{k_s} = \frac{5.993 \times 10^{-13}}{d_{50}} \frac{1 - 0.277 k_n/k_s}{k_s/k_n - 0.259} \tag{5}$$

$$\nu = \frac{0.78 - 0.1156 k_s/k_n}{1 + 3.80 k_s/k_n} \tag{6}$$

where k_s and k_n are the tangential and normal stiffness (N/m), respectively; and $d_{50} = 0.0013$ m is the average diameter of the assemblage included to unify the units at both sides of the equations.

With regard to tensile strength, the relationship between macroscopic tensile strength (σ_t) and bond tensile strength (R_t) is established considering that the sample failure mainly results from the tensile failure of the contact bonds. A linear relation is observed in Fig. 10 and expressed as follows:

$$\sigma_t = R_t \Big/ \left(1716.6 d_{50}^2\right) \tag{7}$$

where R_t is the bond tensile strength in N.

With regard to compressive strength, it is difficult to give a theoretical solution due to the complex micro-mechanisms. According to the analysis and speculation, the unconfined compressive strength (σ_c) is related to both the stiffness ratio and the bond strength ratio (i.e. R_t/R_c). Analysis of the strength envelope in Fig. 6 and the simulation results indicate that the unconfined compressive strength is in linear relation with the bond tensile strength or bond compressive strength with other microscopic parameters fixed. With the assumption that the rock sample loses its strength when the bond strength is 0, the expression can be written as follows:

$$\sigma_c = k R_t \tag{8}$$

The relationship between the parameter k in Eq. (8) and R_t/R_c was then investigated under different values of k_s/k_n (Fig. 11). As illustrated in Fig. 12, k decreases with increasing R_t/R_c at fixed k_s/k_n in a similar manner regardless of different values of k_s/k_n ranging from 0.3 to 0.9. Thus, for simplification, k can be approximated by the following equation:

$$k = \frac{2.6533 \times 10^{-9} - 3.887 \times 10^{-10} \ln(R_t/R_c)}{d_{50}^2} \tag{9}$$

By substituting Eq. (9) into Eq. (8), the relationship between the unconfined compressive strength and the microscopic parameters is obtained as follows:

$$\sigma_c = \frac{[26.533 - 3.887 \ln(R_t/R_c)] R_t \times 10^{-10}}{d_{50}^2} \tag{10}$$

3.4. Changing laws of microscopic parameters due to weathering

The relations between the microscopic parameters and weathering time are obtained by substituting Eqs. (5), (6) and (7) into Eqs.

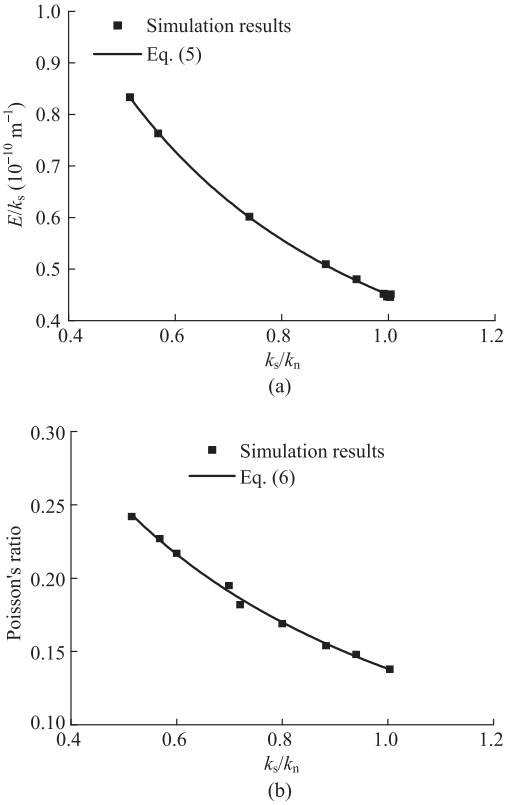

Fig. 9. Relationships between (a) the ratio of elastic modulus to tangential stiffness, E/k_s, and stiffness ratio, k_s/k_n, and (b) Poisson's ratio, ν, and stiffness ratio, k_s/k_n.

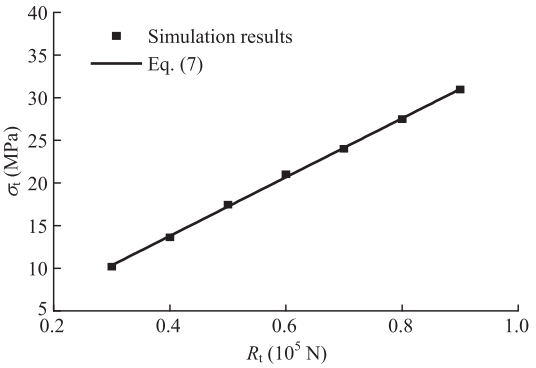

Fig. 10. Relationship between tensile strength σ_t and bond tensile strength R_t.

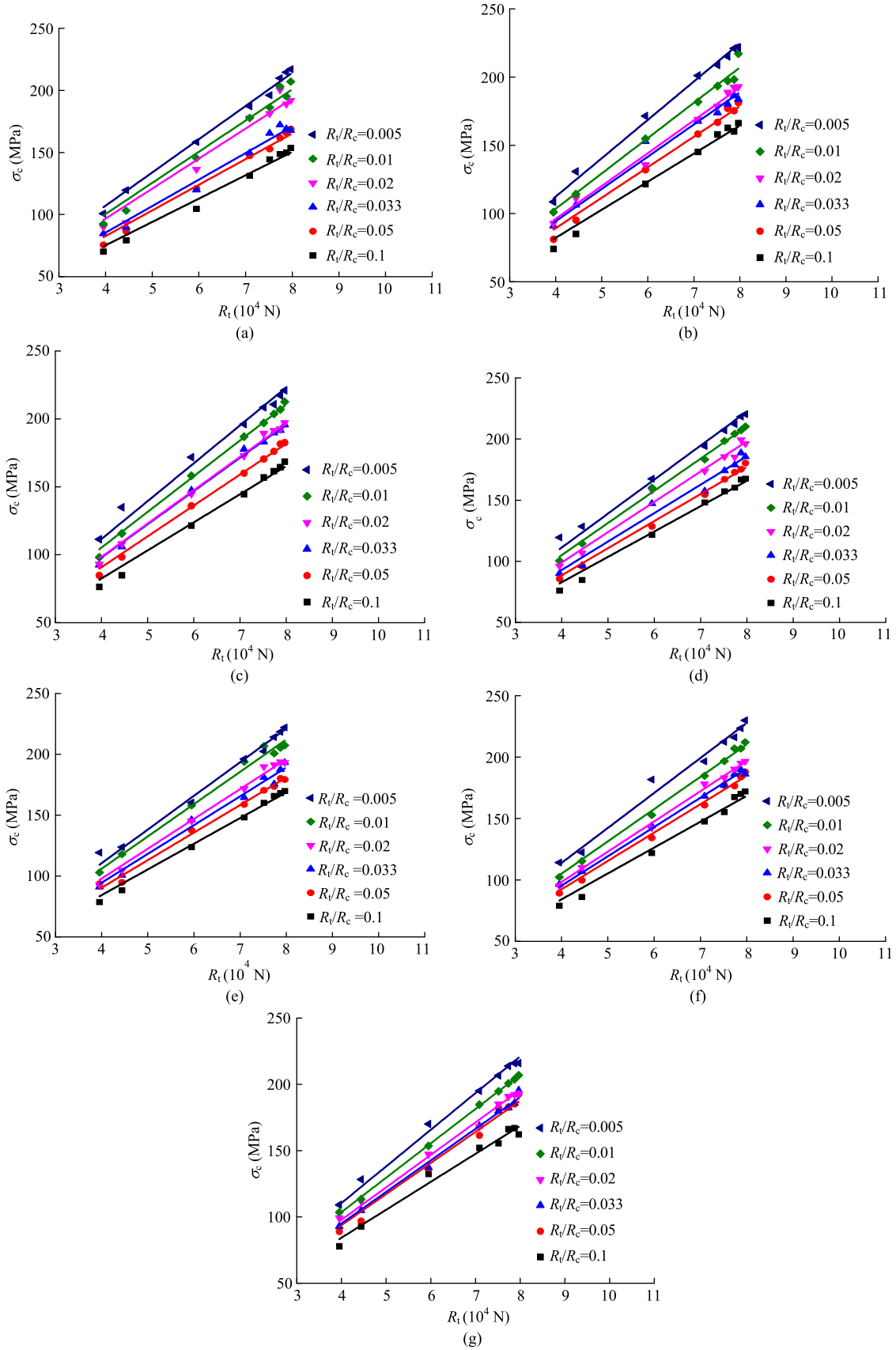

Fig. 11. Relationships between unconfined compressive strength, σ_c, and bond tensile strength, R_t, when (a) $k_s/k_n = 0.3$; (b) $k_s/k_n = 0.4$; (c) $k_s/k_n = 0.5$; (d) $k_s/k_n = 0.6$; (e) $k_s/k_n = 0.7$; (f) $k_s/k_n = 0.8$; and (g) $k_s/k_n = 0.9$.

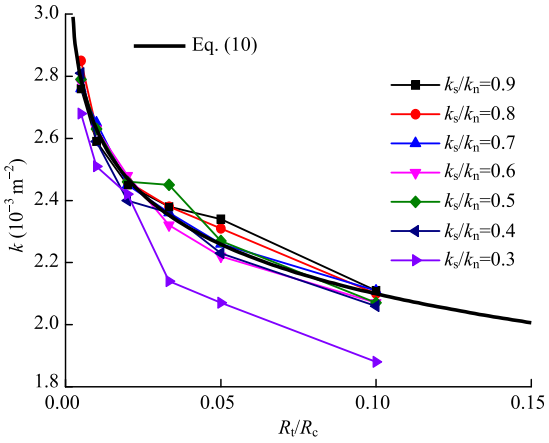

Fig. 12. Relationship between k in Eq. (8) and R_t/R_c under different values of k_s/k_n.

(3), (4) and (2), respectively. The expressions are written as follows with the same units as mentioned above:

$$R_t = 1716.6 d_{50}^2 \sigma_{t0} e^{-0.0643t} \tag{11}$$

$$\frac{k_s}{k_n} = \frac{5.9 - 0.0583t}{8.376 + 0.2154t} \tag{12}$$

$$k_n = \frac{d_{50} E_0 e^{-0.066t} (k_s/k_n - 0.259)}{5.993 \times 10^{-13} (k_s/k_n - 0.277)} \tag{13}$$

In addition, the relation between R_t/R_c and weathering time is obtained by substituting Eqs. (1) and (11) into Eq. (10):

$$\frac{R_t}{R_c} = \exp\left(6.826 - \frac{1.499\sigma_{c0} e^{-0.0404t}}{\sigma_{t0} e^{-0.0643t}}\right) \tag{14}$$

Based on Eqs. (11)–(14), the microscopic parameters required by DEM analyses can be achieved at any given weathering time, strength and elastic modulus of unweathered rock.

It is also indicated from Eqs. (11)–(14) that k_n, R_t and R_t/R_c present exponential relations with weathering time, while the relation between k_s/k_n and weathering time is a fractional function. Fig. 13 shows the variation rules of two critical microscopic parameters, i.e. the stiffness ratio k_s/k_n and the strength ratio R_t/R_c. All these microscopic parameters are in qualitative agreement with the macroscopic changing laws that exhibit degradations in decreasing rates with increasing weathering time. It is noted that R_t/R_c decreases faster than R_t, resulting in a higher decreasing rate of R_t than R_c, which is consistent with the fact that the tensile strength of rocks deteriorates faster than the compressive strength.

4. DEM modeling of weathered rock

The evolution laws of the microscopic parameters due to weathering were implemented here to investigate the effect of weathering on the mechanical properties of rocks.

4.1. Modeling procedure

Weathering is a continuous and slow process, and its impact on rock behaviors can hardly be detected in a short period of time. Nevertheless variation is relatively notable at the initial stage of weathering. Accordingly, different weathering times of 0 ka, 0.1 ka, 0.2 ka, 0.5 ka, 1 ka, 2 ka, 5 ka, 10 ka and 12 ka were selected for DEM

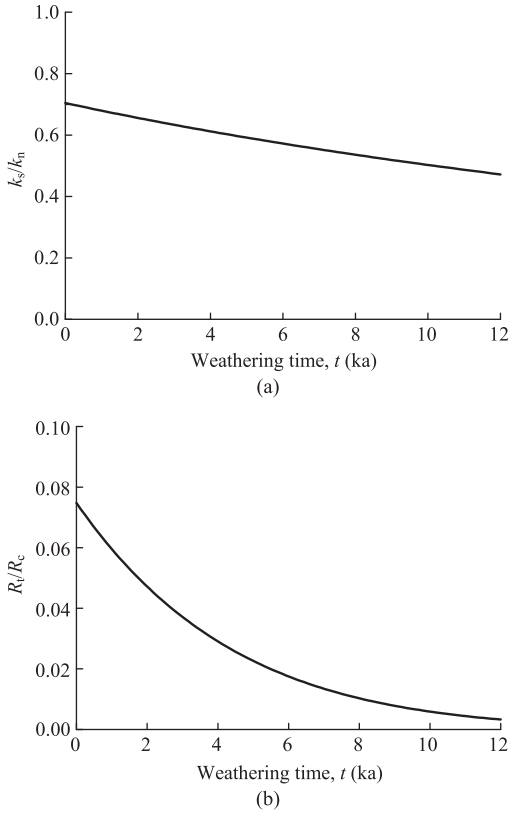

Fig. 13. Changing laws of microscopic parameters in terms of (a) k_s/k_n and (b) R_t/R_c.

simulations of uniaxial compression tests and direct tension tests on weathered rock samples. During the simulations, macroscopic mechanical properties were monitored in comparison with the analytical results. The compressive and tensile strengths were computed from the unbalanced forces on top and bottom of the sample averaged by the sample width. The elastic modulus was inferred from the slope of the initial linear segment of the stress–strain curve. The Poisson's ratio was calculated by the ratio of the incremental lateral strain to the incremental axial strain.

4.2. Comparison with analytical results

The results obtained from DEM simulations with the microscopic parameters determined by Eqs. (11)–(14) are compared to the analytical results using Eqs. (1)–(4) for validation of the changing laws of microscopic parameters due to weathering (Fig. 14). Fig. 14a and b shows that the deformation parameters including elastic modulus and Poisson's ratio obtained from simulations and calculations are consistent in variation trend, and minor discrepancies occur (within 9% and 7% in the case of elastic modulus and Poisson's ratio, respectively). As shown in Fig. 14c and d, the simulated strengths decrease with increasing weathering time, which are also in good agreement with the calculated results (error within 2% and 7% in the case of unconfined compressive strength and tensile strength, respectively).

In general, the simulations are able to capture the fundamental changing laws of the parameters. However, some discrepancies occur, which are mainly attributed to the simplifications during the establishment of the changing laws of microscopic parameters. Actually, it is challenging to establish an exact correspondence between the DEM microscopic parameters and the macroscopic properties.

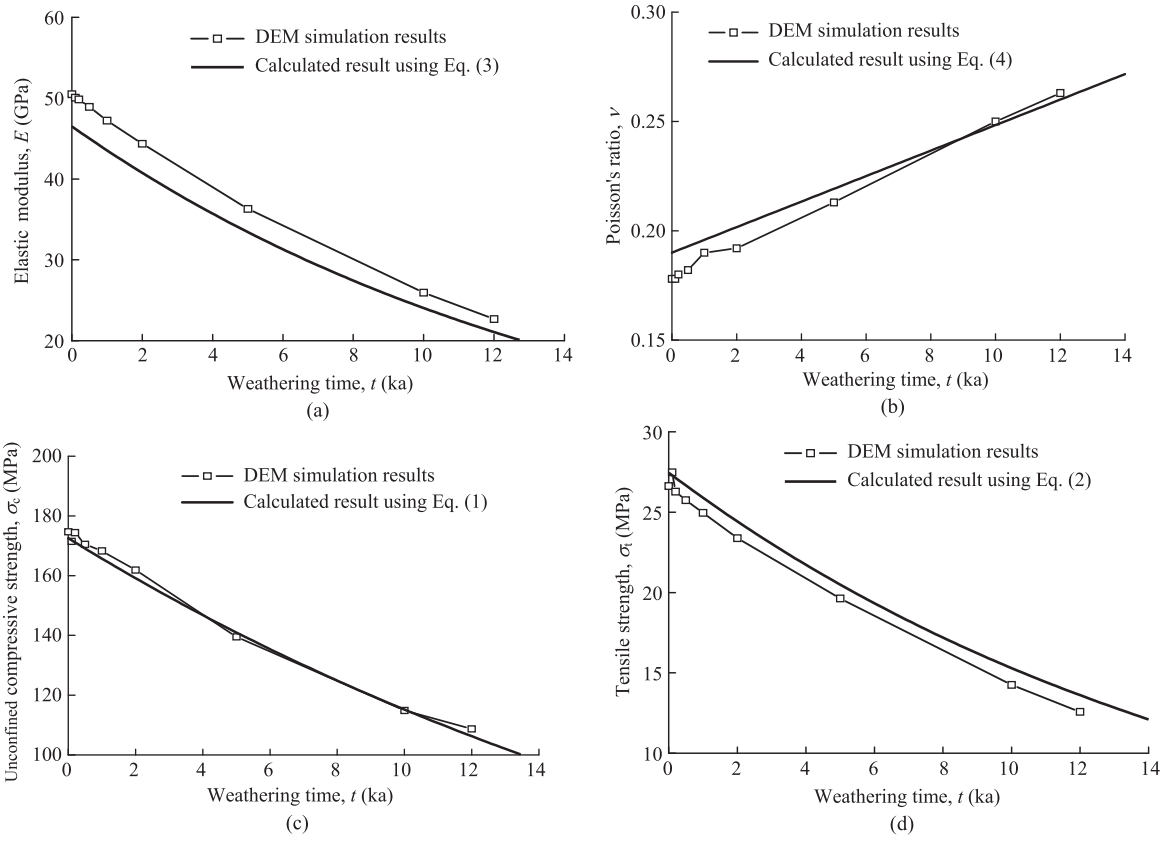

Fig. 14. DEM simulated and calculated results of (a) elastic modulus; (b) Poisson's ratio; (c) unconfined compressive strength; and (d) tensile strength.

4.3. *Effect of weathering*

In contrast to compression tests, the weathering time has an insignificant effect on the rate and distribution of bond breakage under tension tests, although it does affect the tensile strengths of the samples as shown in Fig. 14d. Therefore, this section only presents the DEM results of the uniaxial compression tests on unweathered and weathered rock samples at the weathering times of 0 ka, 2 ka, 5 ka, 10 ka and 12 ka to illustrate the variation of microscopic properties owing to weathering.

The stress–strain relations obtained from DEM simulation of uniaxial compression tests (Fig. 15a) exhibit typical features of rocks. The elasticity and the rigidity of the rock are reflected by the initial linear stage and the small strain at the peak strength, respectively, which are not affected by weathering. However, weathering gradually increases the strain when the peak strength is reached (from approximately 0.35% to 0.5%, corresponding to weathering time of 0–12 ka) in addition to the reduction of strength and elastic modulus of the rock samples. This is because the contact stiffness between rock grains decreases with the increase of weathering time. It leads to a degraded elastic modulus of the assembly, which enlarges the strain at the peak strength. In addition, for unweathered rock, the stress drops rapidly after its peak, while along with the weathering progress, a fluctuation

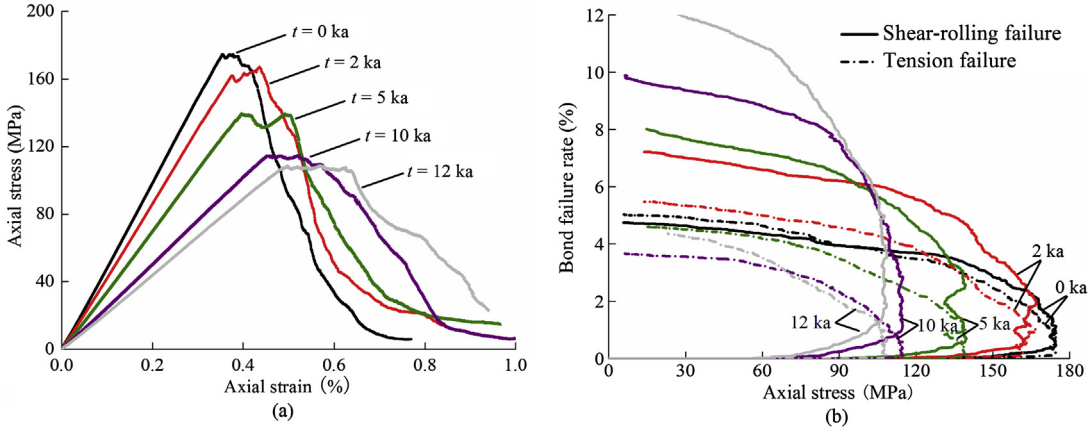

Fig. 15. DEM simulated results of uniaxial compression tests: (a) stress–strain relations; and (b) bond failure rate–strain relations.

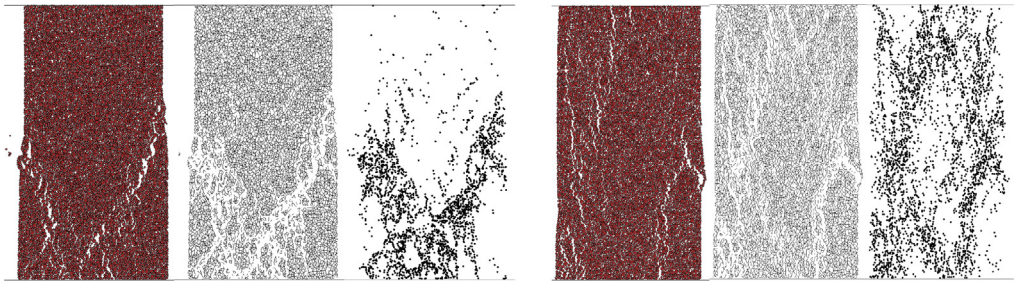

Fig. 16. Diagrams of (from left) post-failure DEM rock sample, bond network and failed bond distribution for (a) unweathered rock and (b) weathered rock.

phase that delays the stress drop becomes significant. The bond failure rate–strain relations (Fig. 15b) indicate the macroscopic failures of the rock samples, from a microscopic level, are resultant from the abrupt increases of the contact bonds. The shear-rolling failure rates of both unweathered and weathered rock samples are basically consistent, while tension failure plays a more crucial role in comparison with shear-rolling failure in the case of weathered rock sample, where the tension failure rate corresponding to the peak axial stress and its range of abrupt increase are much larger than those of unweathered sample.

Fig. 16 presents the post-failure DEM rock samples, bond networks and failed bond distributions of unweathered and weathered rocks. Under the same axial strain, weathered rock sample (Fig. 16b) exhibits a more fragmentized condition with several near-vertical cracks, while two main inclined failure planes are developed in unweathered rock sample (Fig. 16a). The failed bond distributions also show that in weathered rock sample, bond failure is more dispersed within the entire sample, while it is partially distributed in the unweathered rock. In general, weathering has notable effects on the stress–strain relation and failure patterns of the rock sample.

5. Conclusions

This study introduces weathering factor into a DEM bond contact model recently developed by Jiang et al. (2013) for rocks to establish the changing laws of the microscopic parameters in DEM simulation. A series of DEM simulations of the weathered rock samples is conducted to analyze the effects of weathering from microscopic point of view. Major conclusions are drawn as follows:

(1) An exponential function can generally feature the changing laws of strength and elastic modulus of rocks due to weathering, although the constants in the functions may be affected by rock lithology and weathering environment.
(2) The changes of microscopic parameters derived from a parametric study of DEM simulations are found to be consistent with those of macroscopic properties.
(3) The comparisons between the simulations of unweathered and weathered rock samples demonstrate that weathering has notable effects on both stress–strain relation and failure patterns of the rock sample. The rate of tension failure plays a more crucial role than shear-rolling failure in the weathered sample. And the rate of tension failure is different for unweathered and weathered rock samples.

Conflict of interest

The authors wish to confirm that there are no known conflicts of interest associated with this publication and there has been no significant financial support for this work that could have influenced its outcome.

Acknowledgments

The research was funded by the National Basic Research Programs of China (Grant Nos. 2011CB013504 and 2014CB046901), the National Funds for Distinguished Young Scientists of China (Grant No. 51025932), and the National Nature Science Foundation of China (Grant No. 41372272). All these supports are highly appreciated.

References

Beavis FC, Roberts FI, Minskaya L. Engineering aspects of weathering of low grade metapelites in an arid climatic zone. Quarterly Journal of Engineering Geology 1982;15(1):29–45.
Calvetti F, Nova R, Castellanza R. Weathering of soft rocks: continuum and discrete approaches. In: Proceeding of the International Conference on Powders and Grains 2005. London: Taylor & Francis Group; 2005. p. 665–9.
Cundall PA, Strack ODL. A discrete numerical model for granular assemblies. Geotechnique 1979;29(1):47–65.
Griffiths DV, Mustoe GGW. Modelling of elastic continua using a grillage of structural elements based on discrete element concepts. International Journal for Numerical Methods in Engineering 2001;50(7):1759–75.
Gupta AS, Rao KS. Index properties of weathered rocks: inter-relationships and applicability. Bulletin of Engineering Geology and the Environment 1998;57(2):161–72.
Gupta AS, Rao KS. Weathering effects on the strength and deformational behavior of crystalline rocks under uniaxial compression state. Engineering Geology 2000;56(3–4):257–74.
Hachinohe S, Hiraki N, Suzuki T. Rates of weathering and temporal changes in strength of bedrock of marine terraces in Boso Peninsula, Japan. Engineering Geology 2000;55(1–2):29–43.
Irfan TY, Dearman WR. Engineering classification and index properties of a weathered granite. Bulletin of the International Association of Engineering Geology 1978;17(1):79–90.
Jiang MJ, Konrad JM, Leroueil S. An efficient technique for generating homogeneous specimens for DEM studies. Computers and Geotechnics 2003;30(7):579–97.
Jiang MJ, Sun YG, Li LQ, Zhu HH. Contact behavior of idealized granules bonded in two different interparticle distances: an experimental investigation. Mechanics of Materials 2012;55:1–15.
Jiang MJ, Yu HS, Harris D. Bond rolling resistance and its effect on yielding of bonded granulates by DEM analyses. International Journal for Numerical and Analytical Methods in Geomechanics 2006;30(8):723–61.
Jiang T, Jiang MJ, Chen H, Liu F, Shi ZM. A novel bond contact model for rock and its calibration. In: Geotechnical safety and risk IV. Hong Kong: CRC Press; 2013. p. 385–90.
Kimmance GC. Computer aided risk analysis of open pit mine slopes in kaolin mined deposits. PhD Thesis. London: University of London; 1988.
Matsukura Y, Hashizume K, Oguchi CT. Effect of microstructure and weathering on the strength anisotropy of porous rhyolite. Engineering Geology 2002;63(1–2):39–47.
Minh NH, Cheng YP. DEM investigation of the effect of particle-size distribution on one-dimensional compression. Geotechnique 2013;63(1):44–53.
Morgan JK. Numerical simulations of granular shear zones using the distinct element method: 2. Effects of particle size distribution and interparticle friction on mechanical behavior. Journal of Geophysical Research: Solid Earth (1978–2012) 1999;104(B2):2721–32.

Oguchi CT, Hatta T, Matsukura Y. Weathering rates over 40000 years based on changes in rock properties of porous rhyolite. Physics and Chemistry of the Earth, Part A: Solid Earth and Geodesy 1999;24(10):861–70.
Potyondy DO, Cundall PA. A bonded-particle model for rock. International Journal of Rock Mechanics and Mining Sciences 2004;41(8):1329–64.
Shimizu H, Murata S, Ishida T. The distinct element analysis for hydraulic fracturing in hard rock considering fluid viscosity and particle size distribution. International Journal of Rock Mechanics and Mining Sciences 2011;48(5):712–27.
Sunamura T. A physical model for the rate of coastal tafoni development. The Journal of Geology 1996;104(6):741–8.
Tugrul A. The effect of weathering on pore geometry and compressive strength of selected rock types from Turkey. Engineering Geology 2004;75(3–4):215–27.
Utili S, Nova R. DEM analysis of bonded granular geomaterials. International Journal for Numerical and Analytical Methods in Geomechanics 2008;32(17):1997–2031.
Wang Y, Tonon F. Modeling Lac du Bonnet granite using a discrete element model. International Journal of Rock Mechanics & Mining Sciences 2009;46(7):1124–35.
Wiącek J, Molenda M. Microstructure and micromechanics of polydisperse granular materials: effect of the shape of particle size distribution. Powder Technology 2014;268:237–43.

Dr. Mingjing Jiang is a professor of civil engineering at Tongji University, and the Vice President of ISSMGE Technical Committee 105 (Geomechanics from Micro to Macro). Prof. Jiang received his Ph.D. in Nanjing Hydraulic Research Institute in 1996. Before he joined Tongji University in 2006, Dr. Jiang worked as a research fellow in Geo-research Institute and Kyoto University, Japan from 1998 to 2000, and as a postdoctoral fellow in Laval University, University of Manchester, and University of Nottingham from 2000 to 2006. Dr. Jiang's research interests cover the geomechanics from micro to macro for problematic geomaterials (e.g. structural sands, loess, soft soils methane hydrate bearing sediments, lunar soils, soft rocks), and DEM application to geo-engineering. Prof. Jiang is the Laureate of China National Funds for Distinguished Young Scientists. He is the editorial board member of 5 international journals including Granular Matter, Computers and Geotechnics, and Transportation Geotechnique. He published 2 books and about 300 journal papers and peer-reviewed conference papers, including one ESI Highly Cited Paper. He received over 660 citations and his H-index is 13 according to Web of Science Citation Reports (Science Citation Index Expanded database).